Journal of Rubber Research (2021) 24:301–318
https://doi.org/10.1007/s42464-020-00071-7

REVIEW

Elastomeric door seal analysis under aircraft cabin pressure

B. Franke Goularte[1] · V. Zatko[1] · A. Lion[1] · M. Johlitz[1]

Received: 8 June 2020 / Accepted: 14 December 2020 / Published online: 1 February 2021

Abstract
Simple strategies are used to physically represent the cabin pressure acting on elastomeric seals for aircraft door applications. The relationships between rubber response, contact problem and air pressure are assumed as the initial step to understand the risks of air leakage during the early stages of a flight cycle. Through the finite element method, the non-linear boundary problem is investigated with the distinct contact response from two types of door interfaces. The options available within the ABAQUS commercial software are explored to model the seal as nearly incompressible, whereby the limitations are compared for each solution. In a qualitative approach, the simulations use the contact pressure distributions to define the pressure load for air leakage investigations on the door corners.

Keywords FEM · Elastomeric aircraft door seal · Cabin pressure · Air leakage · ABAQUS

Introduction

During an aircraft flight, the pressure difference between the cabin and the outer atmosphere generates distributed loads which need to be withstood by the fuselage and the cutout structures. Around the contours of aircraft doors, gaps are necessary to accommodate the kinematics of the opening and closure mechanisms. In order to keep the air pressure for breathable human conditions, elastomeric seals solutions are added to the aircraft doors to avoid air leakage.

Figure 1 illustrates how the cabin differential pressure load is ideally distributed over the seal cross section and the surrounding door structures. Inflatable design solutions are generally employed since they take advantage of the positive pressure by adding vent holes to increase the contact forces with the mating interface. Elastomers have been primarily employed for seal door systems due to their intrinsic ability to take shape from their mating interface when subjected to large deformations. The hyperelastic behaviour and the nearly incompressible nature of rubber play an essential role in sealing performance. In its attempt to return to the initial configuration, an elastomeric seal can reach the sealing effect, if the contact pressures remain higher than the fluid pressure over the contact boundaries [8]. Predicting the risks of air leakage under cabin differential pressure is essential to guarantee the seal functionality.

In an ideal door system, the contact stress distribution between the seal and the striker interface should be as independent as possible from all external disturbances. Since the seal profiles are inserted into the specified radii and door contours, some points can arise where the sealing line is no longer locally stable, which also affects the contact pressures and thus the final sealing effect. In such conditions, the leakage of air is triggered, which can later be traced as a source of aerodynamic noise, vibration and, in critical scenarios, cabin depressurisation [6]. For this reason, the relations between seal, striker and cabin pressure are a piece of crucial information to design an efficient interface.

In an aircraft development, door seals are defined according to the main structural and kinematic elements of the fuselage and the door mechanisms. It is up to the seal manufacturers to define complex seal profiles made of several different thermally stable elastomers, that are suitable for the sealing interface. They can be either homogeneous or fibre-reinforced, being produced by extrusion or injection techniques, and further combined with coating layers to reduce friction between mating components. Prototyping methods in combination with trial and error are not the best options available

Dr Michael Johlitz, Guest Editor of this Special Issue [New Challenges and Methods in Experimental Investigations and Modelling of Elastomers] confirms that where he was co-author of a research article in this Special Issue, he was not involved in either the peer review or the decision-making process of that particular article.

✉ B. Franke Goularte
bruno.franke@unibw.de

[1] Institute of Mechanics, Bundeswehr University Munich, Werner-Heisenberg-Weg 39, 85579 Neubiberg, Germany

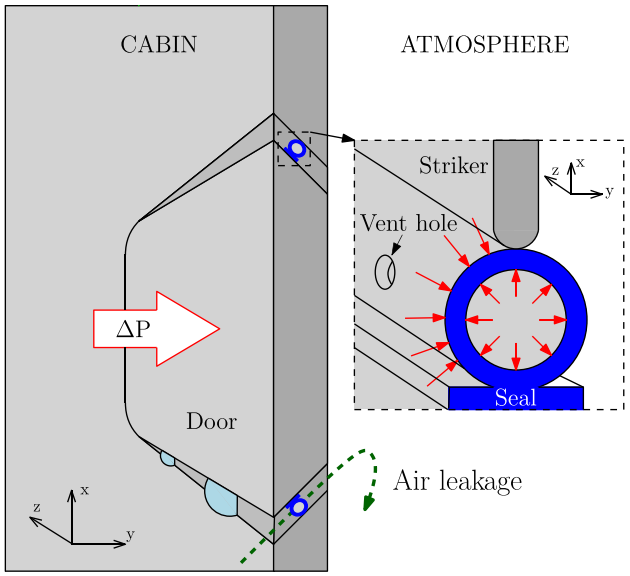

Fig. 1 Load pressure distribution over the door structures

to develop a seal design as they tend to be expensive, time-consuming and end up working as partial design solutions. Therefore, commercial FEM tools have mainly been used by product development engineers to investigate innovative design solutions based on comprehensive material formulations and loading case simplifications of real conditions.

With help from ABAQUS/CAE 2018 commercial software, the simulations are conducted with distinct strikers and a customised seal profile to understand the pressure problem. Pure hyperelastic behaviour is assumed to simplify the model in a qualitative approach to analyse the door seal response regarding contact pressure in the corner locations. In the model definition and analysis sections, the essential hyperelastic material formulation is revisited to discuss further aspects of handling the internal incompressible constraint depending on the solver scheme. Element mesh refinement studies are presented for maximum strain, compressive forces and contact pressure, based on Grid Convergence Index criteria, commonly seen in the literature [14].

The relevant researched topics that supported this article are summarised in the next section entitled State of the art. Several different load scenarios and material aspects of rubber seals are not fully covered in this paper. However, the complex coupling between pressure load and contact interactions for general non-linear FEM problems is a necessary initial model set-up to evaluate how the air leakage is originated in the seals.

State of the art

Predicting the risks of air leakage on an elastomeric seal requires a physically comprehensive material modelling for rubber and a reliable method to prescribe the fluid pressure. Typically, the fluid-media compatibility of aerospace rubber seals permits nitrile, silicone, and fluorosilicone elastomers according to seal manufacturers [12, 20]. The stress response of such rubber-like materials can be strongly history-dependent, leading to relaxation of the contact forces with time [1]. High and low temperatures can influence the mechanical properties of reinforced rubber [7], typically applied for inflatable seal designs [16]. The presence of chemical contaminants can also degrade the elastomer network in an ageing process, modifying the mechanical behaviour for materials such as nitrile rubber [10].

Initial seal performance investigations can be traced back to the O-rings failure report of the space shuttle Challenger disaster in 1986 [15]. FEM analysis was applied to predict the gasket joints deformations in contact with rigid metallic interfaces for rocket boosters considering temperature influence [18]. Experimental investigations of elastic leakage [8] and fluid percolation [13] show, at different scales, how the seal performance depends on contact pressure distribution. More advanced numerical techniques such as computational fluid dynamics (CFD) [1] and coupled Euler Lagrangian (CEL) [9] were used to simulate fluid-structural interactions between liquid pressure and seal behaviour in post-leak conditions. On the shape optimisation level, parametric studies with swellable elastomeric seals highlight the potential of minimising the leakage [3] by finding the interface which maximises contact pressures.

For aircraft door seal applications, the FEM analysis performed by Zhao [22] features a simplistic approach to prescribe the cabin pressure load with fluid pressure penetration (FPP) interaction, at the expense of neglecting the air leakage quantification. In this case, a pre-defined contact pair interaction is used to define pressure load conditions and evaluate the seal performance. However, ABAQUS offers this feature for specific implicit solutions, which requires attention to possible convergence issues due to contact interactions, large deformations, complex loading conditions and material non-linearities. In a quasi-static approach, explicit solutions can be applied to overcome convergence difficulties and remain close to the static implicit solver results, depending on loading speed, seal degree of confinement and material density, as studied by Yurdabak [21] for rubbers. Thus, an alternative strategy is envisaged by defining distributed loads through the explicit subroutine VDLOAD [5] based on a contact boundary.

FEM model definitions

This section defines the model assumptions employed to the equilibrium equations and material formulations that are essential for the displacement-based finite element method of analysis for seal performance investigations. The seal is

modelled as a non-linear elastic body following the constitutive relations for hyperelastic incompressible and nearly incompressible behaviour. For the sake of simplification, the striker interface is interpreted as a discrete rigid part since the metallic components are much stiffer than the rubber seal. The boundary value problem is initially defined by the interactions between seal, striker and air pressure. By assuming quasi-static loading conditions during the early stages of flight, the analysis is performed in two steps of door kinematics and cabin pressurisation.

The risks of leakage are assumed to take place during the climb phase, after relatively long periods between aircraft taxiing and take-off, by neglecting large variations of the seal stress response due to temperature and stress relaxation. The complete flight load-temperature spectrum of the seal is not considered in the analysis. Nevertheless, the hypotheses of isothermal and quasi-static loadings are not far from the real conditions of full-scale static tests performed with aircrafts on ground for certification. Further aspects such as thermo-viscoelasticity, thermal strains and ageing effects shall enrich the simulations, but these premises are simplified so that analyses of sealant interfaces are carried out qualitatively.

Equilibrium equations

Following the assumptions, the equilibrium equations and material behaviour of rubber are described based on the conservation of energy implied by the laws of thermodynamics. The fundamental virtual work principle is described in the Eulerian formulation:

$$\int_{\Omega} \boldsymbol{\sigma} : \delta\mathbf{D}\mathrm{d}v = \int_{\Gamma} \mathbf{t} \cdot \delta\mathbf{v}\mathrm{d}s + \int_{\Omega} \mathbf{f} \cdot \delta\mathbf{v}\mathrm{d}v, \tag{1}$$

where $\delta\mathbf{v}$ is the virtual velocity vector of the body, and $\mathbf{t}$, $\mathbf{f}$ are the surface traction and body forces, respectively integrated over the boundary Γ and over elastic body volume Ω. The left-hand side of this equation expresses the internal virtual work rate in terms of Cauchy stress $\boldsymbol{\sigma}$ and the conjugate strain rate $\mathbf{D}$. Assuming the compatibility with the kinematic constraint that satisfies $\delta\mathbf{v} = 0$ on Γ, the traction $\mathbf{t}$ is split into surface distributed pressure loads $\mathbf{t}^F$ and contact traction constraints $\mathbf{t}^C$:

$$\int_{\Gamma} \mathbf{t} \cdot \delta\mathbf{v}\mathrm{d}s = \int_{\Gamma_F} \mathbf{t}^F \cdot \delta\mathbf{v}\mathrm{d}s + \int_{\Gamma_C} \mathbf{t}^C \cdot \delta\mathbf{v}\mathrm{d}s. \tag{2}$$

Figure 2 illustrates how the distributed pressure load is defined in two domains ($\Gamma_F = \Gamma_{F_1} \cup \Gamma_{F_2}$), where Γ_{F_1} is delimited by the contact boundary Γ_C and Γ_{F_2} is located on the hollow inflatable surface of the seal, by considering the existence of vent holes along the cross-section. The traction on the contact boundary $\mathbf{t}^C$ is derived from normal and tangential frictional components that are dependent on the

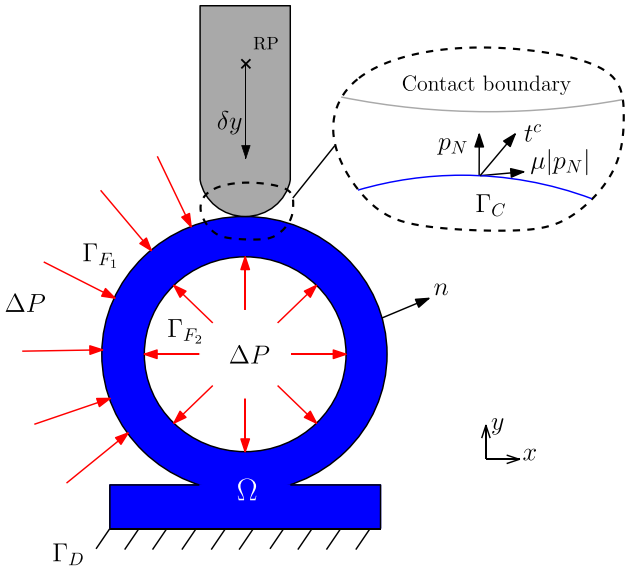

Fig. 2 General seal body with frictional contact and a rigid striker with boundary loading conditions

contact pressure p_N computed by penalty method. Lastly, the coefficient of friction μ relates normal nodal traction components with the tangential contact forces.

Material law

The elastic behaviour considering a homogeneous seal section is expressed by a hyperelastic constitutive law, generally applied for rubber-like materials. By considering the existence of a free energy density function of Helmholtz ($\psi = e - \eta\theta$), where e is the internal energy of the system and η is the entropy density multiplied by the absolute temperature θ of the body, the Clausius–Duhem inequality is presented relative to the current configuration:

$$-\rho\dot{\psi} + \boldsymbol{\sigma} : \mathbf{D} - \rho\eta\dot{\theta} - \frac{1}{\theta}\mathbf{q} \cdot \mathbf{grad}_{\mathbf{x}}(\theta) \geq 0, \tag{3}$$

where ρ is the material density belonging to the current configuration and $\mathbf{q}$ is the heat flux vector. By imposing isothermal boundary conditions, the Cauchy stress tensor $\boldsymbol{\sigma}$ and the strain rate tensor $\mathbf{D}$ are the remaining variables of the Clausius-Planck inequality:

$$-\rho\dot{\psi} + \boldsymbol{\sigma} : \mathbf{D} \geq 0. \tag{4}$$

In the case of hyperelasticity, the left Cauchy–Green strain tensor $\mathbf{B}$ is selected as the process variable of the free energy function ψ. For a homogeneous isotropic solid, the time derivative of the free energy is written as a function of principal strain invariants:

$$\dot{\psi} = \frac{\partial \psi}{\partial \mathbf{B}} : \dot{\mathbf{B}} = \left(\frac{\partial \psi}{\partial I_1}\frac{\partial I_1}{\partial \mathbf{B}} + \frac{\partial \psi}{\partial I_2}\frac{\partial I_2}{\partial \mathbf{B}} + \frac{\partial \psi}{\partial I_3}\frac{\partial I_3}{\partial \mathbf{B}} \right) : \dot{\mathbf{B}} \tag{5}$$

where the term $\dot{\mathbf{B}}$ can be re-written by exploiting its relation with the gradient of deformation $\mathbf{F}$ and the decomposition of the symmetric part of the spatial velocity gradient $\mathbf{L}$ into the strain rate tensor $\mathbf{D}$ found more in detail in [4].

$$\dot{\mathbf{B}} = \mathbf{L} \cdot \mathbf{B} + \mathbf{B} \cdot \mathbf{L}^T \tag{6}$$

By assuming a homogeneous seal section without fiber reinforcements, the energy function is considered isotropic. So the hyperelastic constitutive law is given by the stress-strain relation, also described by [17]:

$$\boldsymbol{\sigma} = 2\rho \mathbf{B} \cdot \frac{\partial \psi}{\partial \mathbf{B}} \tag{7}$$

This equation enables to describe a reversible, rate independent, non-linear material behaviour on the current configuration with the strain invariants:

$$\begin{aligned} I_1 &= \mathrm{tr}(\mathbf{B}), \\ I_2 &= \mathrm{tr}(\mathrm{cof}(\mathbf{B})), \\ I_3 &= \det(\mathbf{B}). \end{aligned} \tag{8}$$

The hypothesis of incompressibility and nearly incompressibility is considered for the rubber seal. In mechanics, the relation between the volume dV in the undeformed configuration to the volume dv in the deformed configuration holds as $\mathrm{d}v = J\mathrm{d}V$, where J is the Jacobian. By assuming elementary volume constancy along with body configurations variations, an internal constraint is established from the relation between J with the third invariant, which holds $J = \sqrt{I_3} = 1$. It requires a reformulation of the free energy function to enforce the local incompressibility condition by introducing a Lagrangian multiplier p.

$$\hat{\psi} = \psi(I_1, I_2) - p(J - 1) \tag{9}$$

In the case of incompressibility, a constitutively undetermined pressure p is added and ψ is only a function of I_1 and I_2:

$$\boldsymbol{\sigma} = 2\rho \mathbf{B} \cdot \frac{\partial \hat{\psi}}{\partial \mathbf{B}} - p\mathbf{I} \tag{10}$$

Essentially, pressure does not affect strain values. The problem by adding this internal constraint is that the solution is no more uniquely dependent on the deformations because the diagonal stress terms can be modified for any values of strain.

To overcome this issue, ABAQUS offers a mixed formulation by adding a pseudo-Jacobian $\hat{J}$ that is used in place of the original Jacobian, allowing to rewrite the free energy function in an augmented form:

Table 1 Material parameters and solver analysis settings

ABAQUS	C_{10}	D_1	Seal density (ρ_0)
Solver	(MPa)	(MPa^{-1})	($\mathrm{ton/mm}^3$)
Implicit	1.0	0.00	–
Implicit	1.0	0.05	–
Explicit	1.0	0.05	1E−09

$$\hat{\psi} = \psi(I_1, I_2, \hat{J}) - \hat{p}(J - \hat{J}) \tag{11}$$

This augmented or mixed formulation has some numerical particularities regarding the solver applicability. The Lagrangian multiplier $\hat{p}$ interpolation for fully incompressible behaviour is only enforced by the hybrid element family, e.g. C3D8H and CPE4H, which is only available on the implicit solver. For most element types, the pseudo-Jacobian is interpolated independently in each element, which can be used for any degree of compressibility in an explicit scheme.

Preliminary 2D model studies

In this subsection, the finite element model is substantiated by preliminary studies considering the seal under limit compression conditions. The material model and mesh convergence are evaluated thorough element refinement over the seal cross section using 2D models. In these cases, the elements employed are CPE4H: 4-node bilinear plane-strain quadrilateral with hybrid formulation for hydrostatic pressure. The hyperelastic behaviour is formulated with the neo-Hookean strain energy potential, which is satisfactory for strain levels up to 50% [19]:

$$\psi = C_{10}(I_1 - 3) + \frac{1}{D_1}(J - 1)^2 \tag{12}$$

Table 1 presents the prototypical material parameters for the implicit and explicit solver analyses. Despite the absence of concrete material data for aircraft door seals, the values are within the range employed in similar studies [1, 22].

In Sect. 4, the parameters are revisited in more detail for comparisons between 3D models using implicit and explicit solvers to deal with the incompressible internal constraint.

From industrial references for inflatable hollow profiles [12], the recommended seal deflections are generally found between 15 and 50% with respect to the height of the bulb geometry. In order to verify whether the neo-Hookean material law is suitable for large deformations under compression, the seal cross section is squeezed beyond the maximum recommended values. The standard P-shape[1] geometry is

[1] Seal bulb height = 38.2 mm and thickness = 3.95 mm.

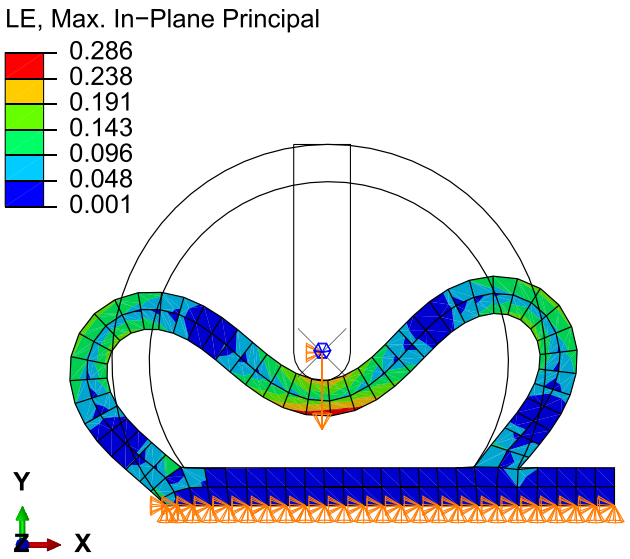

Fig. 3 Logarithmic strain contour results for seal deflection

selected for the seal cross section, being deflected on the y-axis until 65% by the total height of the striker[2]. No cabin pressure is added in the preliminary studies. Only contact interactions between striker and seal are considered for the fully incompressible implicit solutions. The tangential friction coefficient $\mu = 0.4$ is assigned to the contact behaviour for all surfaces pairs, based on relative input values from the reference [9]. Figure 3 shows the contour plot results for maximum logarithmic strain (LE) components of the seal deflection.

By converting the maximum logarithmic strain value of 0.286 to engineering strain, the updated result is read as 33.11%, which is acceptable for the neo-Hookean material law. Although it is satisfactory for the initial verification of the material law, it is necessary to add more elements to the thickness of the seal to capture the bending response. Furthermore, in the presence of contact, the mesh size has a significant influence on the quality of the output results, requiring attention to find a reasonable grid size against CPU time.

The contact pressure values, defined by force per element area, are directly associated with the element length. These values tend to be closer to the exact solution as the ratio of refinement is increased. However, if the number of elements is too high, the calculations necessary for the analysis may take excessive CPU time to finish. Therefore, comparisons between FEM models are typically employed to provide mesh convergence information about the output variables under favourable time steps for the analysis solutions.

[2] Striker length = 25.0 mm and thickness = 6 mm.

The method employed for examining the model outputs and the temporal convergence of the simulations are based on the theory of generalised Richardson's extrapolation, described by Roache [14]. It suggests a Grid Convergence Index (GCI) from a consistent procedure of uniform mesh refinement that verifies if the output results are converging to an extrapolated exact solution. The safety factor of 1.25 is the traditional literature value used to calculate the results within confidence intervals of 95%. For this study, the cross-section of the seal is continuously refined by equal ratios of 2, starting with two elements on the seal thickness cross section (coarse), to four elements (normal), until it reaches eight elements (fine). The convergence check should be close to 1.0 based on the progression of the GCI of each of the three meshes. If this value is out of the interval of 0.9–1.1, the extrapolated exact solution is not recommended to estimate the error. Table 2 presents the results for strain, reaction force and contact pressure on mesh convergence studies.

The striker reaction force and the contact pressure convergence studies are conveniently introduced since they are recalled in other sections. Thus, all compared variables present a convergence check index within the interval of the confidence interval of 95% for GCI. The extrapolated solution with 40.83% maximum strain also suggests that it is feasible to apply the neo-Hookean law. Figure 4 highlights how the variable evolves with the seal section refinement. The arrow vector represents the resultant reaction force (RF), and the contour plot shows the contact pressures (CPRESS) distributed over the sealing surface. The CPU times required for each analysis to finish are 16.2 s (coarse), 30.3 s (normal) and 69.0 s (fine). Based on the convergence studies of 2D models, a reasonable seal mesh refinement for 3D models is proposed to provide analyses under reasonable duration and good compromise with output results.

3D model of door corner

Assuming a similar response of the 2D model studies, the 3D mesh for the seal cross section considers four elements per thickness (normal size) which represents a good agreement between the extrapolated exact solutions and CPU time. From the subsequent analysis, the error of 13.4% associated to the maximum strain is not as relevant as the reaction forces and the contact pressure convergence results, showing, respectively, smaller errors of 1.14% and 2.68%. These output variables are also more relevant for the seal performance investigations and comparisons between striking interfaces. Despite the CPU time not being so critical for 2D simulations, when doubling the duration for each mesh refinement, the finest mesh may be too time-consuming for 3D models, particularly for the explicit scheme.

The element types used for the analysis are dependent on the necessity of using the explicit solution technique

Table 2 Results of element refinement convergence studies

Mesh Size	Max Strain (%)	Index (GCI)	Extrapolated Solution (%)	Error Sol.
Coarse	33.11	23.6%	40.83	18.9%
Normal	36.89	13.4%	40.83	9.66%
Fine	38.82	6.48%	40.83	4.93%
Convergence Check Index			1.052	
Mesh Size	Reaction Force (N)	Index (GCI)	Extrapolated Solution (N)	Error Sol.
Coarse	0.768	4.98%	0.739	3.98%
Normal	0.747	1.41%	0.739	1.14%
Fine	0.741	0.40%	0.739	0.32%
Convergence Check Index			0.992	
Mesh Size	CPRESS (MPa)	Index (GCI)	Extrapolated Solution (MPa)	Error Sol.
Coarse	0.316	50.8%	0.533	40.7%
Normal	0.519	2.68%	0.533	2.68%
Fine	0.532	0.21%	0.533	0.17%
Convergence Check Index			1.025	

rather than implicit time integration schemes due to convergence problems for the pressure loading step. While the C3D8H hybrid element is available for the implicit solver to deal with the incompressibility constraint, the C3D8 standard 8 node linear brick element requires at least a minimum compressible bulk value for the explicit time integration to work. The differences between each solver scheme are observed for the seal response regarding the influence on contact pressure distributions. Far from the door radii contours, 2D FEM models may be useful to approximate the long straight sections of vertical and horizontal parts of the seal. However, at the door corner locations, seal instabilities are more susceptible to exist, due to the intrinsic load path transitions on a sweep seal cross-section. Under cabin pressurisation, a relative sliding movement between mating surfaces can be triggered, if the friction forces are not high enough to hold the seal profile on a stable configuration, due to the tangential and normal contact relationship. It may also influence the sealing effect, giving origin to an air leakage or post-leak effects. Thus, prescribing the pressure load under complex configurations requires attention to the boundary problem.

Two types of striking interfaces are used to address the complexity of defining the coupling between contact interactions and pressure load in three dimensions. Figure 5 shows how the initial boundary conditions are defined to the corner of the seal with the sweep P-shape design and the striker geometries (C-channel and flat surface). The door latching mechanism starts from the zero clearance distance between the mating surfaces. Further boundary conditions are imposed on the seal extremities, as an approximation to the seal section continuity over both the x-axis and z-axis.

For each seal-striker interface, the analysis is performed in two steps. The first load case prescribes the rigid striker displacements to reach an equivalent maximum compressive load on both interfaces. Based on the C-channel striker compression for a limit seal deflection of 65%, the same maximum load is reached for the flat surface when the seal is compressed by 7.5 mm. The second load case considers the seal surfaces under differential cabin pressure during the climb phase. Up to cruise flight conditions at 45,000 ft [11] with a scatter factor of 1.33 for aircraft compartment load requirements [2], the maximum delta pressure of 0.1 MPa is reached. Table 3 summaries, for each striker geometry, the loading steps of compression and pressurisation used to investigate the risks of seal leakage during the early stages of flight, in a quasi-static analysis approach. The impacts of choosing whether perfectly incompressible or nearly incompressible material model are presented for each of the analysis solutions. The material response influences the contact pressure results of the sealing lines, which are essential for the cabin pressure load boundary.

Seal compression: 1st loading step

The numerical solutions available for incompressible and nearly incompressible material behaviour are compared for the seal compression problem regarding the sensitivity to rigid interface design and seal deflection. When the rubber

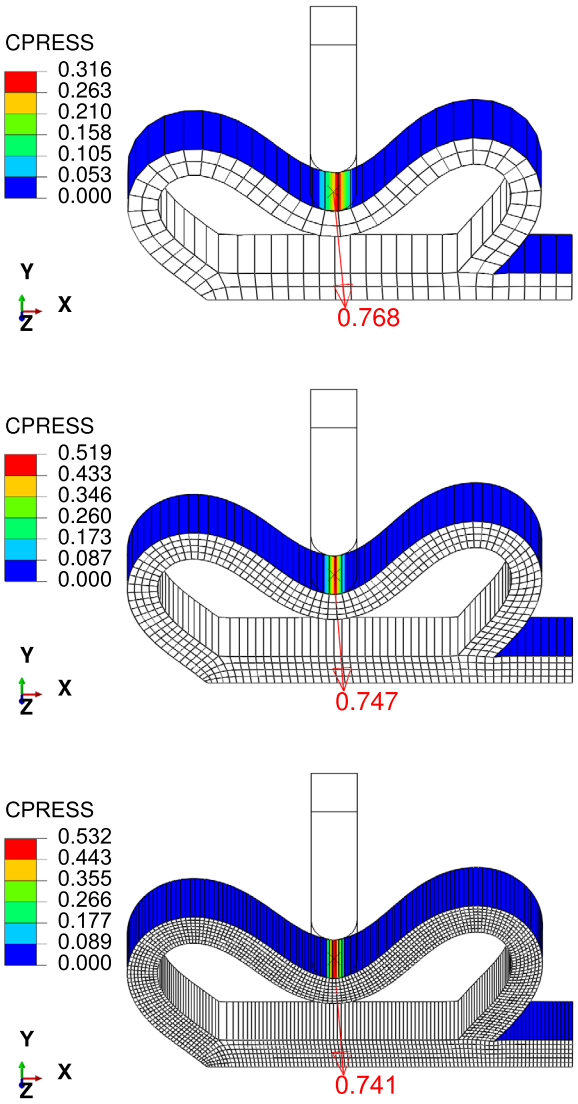

Fig. 4 RF and CPRESS evolution using different mesh sizes

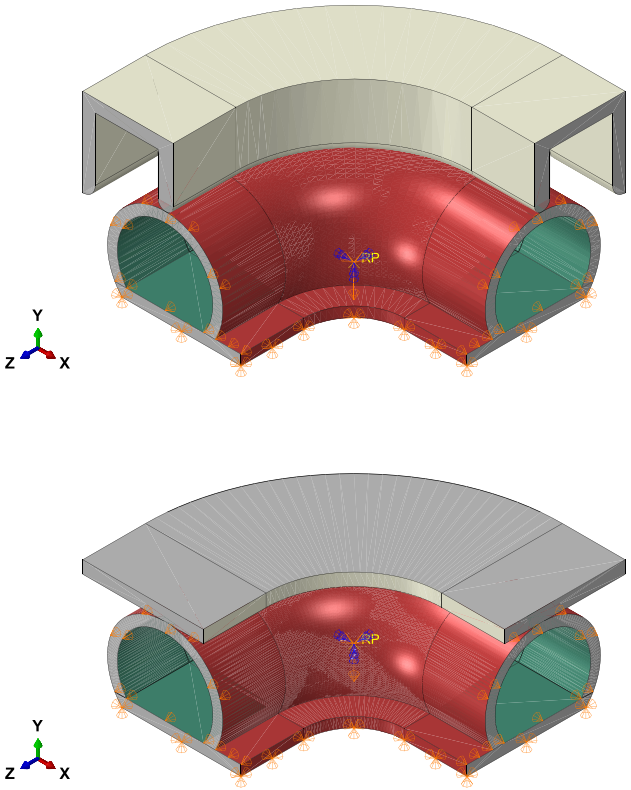

Fig. 5 Door seal corner models with different interfaces

Table 3 Load step analysis for each seal-striker interface

Interface Geometry	Compression 1st step (2s)	Pressurisation 2nd step (1s)
C-channel	− 25.0 mm *Y*-axis	*Δ*P
Flat surface	− 7.50 mm *Y*-axis	0.1 MPa

is highly confined, such as an O-ring, the seal compressibility must be modelled correctly to obtain an accurate bulk response. Due to contact and material non-linearities, the standard implicit solver may present convergence issues for the solution of such problems. Alternatively, the dynamic explicit solver can be used instead in a quasi-static approach of the solution. Therefore, certain remarks regarding the time integration schemes and limitations of the material formulation are given before the comparative results.

Implicit and explicit schemes

For the seal analysis, the load balance between the nodal internal response **I** and the external loads **P** is dependent on the contact forces of the seal compression and the pressure load of cabin pressurisation. Generally, the standard implicit solver performs multiple iterations with Newton's method to balance these non linear equilibrium equations before the solution is reached. The convergence is achieved under contact, residual nodal forces ($\mathbf{R} \approx \mathbf{0}$) and displacement conditions by varying the time increment sizes in smaller fractions. If the increment size is decreased repeatedly, for a maximum number of attempts, the problem could be divergent for the following load balance:

$$\mathbf{P} - \mathbf{I} = \mathbf{R}. \tag{13}$$

For the explicit procedure, inertial forces are added to the load balance, through the nodal mass **M** and the accelerations $\ddot{\mathbf{u}}$. In this type of dynamic integration scheme, also referenced as forwarding Euler method, the convergence is conditioned, since it applies small fixed time increments for the equation:

$$\mathbf{P} - \mathbf{I} = \mathbf{M} \cdot \ddot{\mathbf{u}}. \tag{14}$$

When the right-hand inertial term is small enough, this equilibrium equation can be compared to the static implicit solution. One possibility to mitigate the inertial contribution is by giving long periods for the load prescription, which reduces the accelerations of the problem. Another option is by establishing small masses for the material, which may also increase CPU time due to smaller time increments. In order to keep solver solutions under similar step analysis durations, the material density of rubber is set on the order of 10^{-9} ton/mm^3, remaining closer to real seal properties [20].

Incompressibility constraint limitations

While the implicit standard solution enables the fully incompressible formulation, it is not possible to assume that the material is fully incompressible in the explicit solver. According to ABAQUS manual, the program has no mechanism to impose the incompressibility constraint at each material Gauss point of the elements. A perfectly incompressible material would have an infinite dilatational wave speed c_d, resulting in a time increment Δt of zero [5]. A similar problem also occurs if no material density ρ is assigned, following the time increment definition for the explicit analysis:

$$\Delta t = \frac{L_e}{c_\mathrm{d}}, \qquad c_\mathrm{d} = \sqrt{\frac{\hat{\lambda} + 2\hat{\mu}}{\rho}}, \tag{15}$$

where L_e is the element characteristic length, $\hat{\lambda}$ and $\hat{\mu}$ are the effective Lamé's parameters that can be written in a consistent form with linear elasticity for the material strain energy potential coefficients from the neo-Hookean material law:

$$C_{10} = \frac{\hat{\mu}}{2}, \qquad D_1 = \frac{2}{\hat{\lambda}} \qquad \text{for} \qquad \hat{\mu} \ll \hat{\lambda}. \tag{16}$$

If the bulk compliance D_1 is too small, the scheme requires the use of excessively small time increments and can induce noise on the explicit dynamic solution. Due to this explicit solver limitation, some amount of compressibility must be defined based on analysis results judgment. The terms above are rewritten to express the material compressibility in terms of Poisson's ratio ν by the fractions of the initial bulk modulus K_0 to the initial shear modulus μ_0, as follows:

$$\nu = \frac{3K_0/\mu_0 - 2}{6K_0/\mu_0 + 2}, \qquad K_0 = \frac{2}{D_1}, \qquad \mu_0 = 2C_{10}. \tag{17}$$

An upper limit of 100 is suggested for the ratio of K_0/μ_0 for the ABAQUS explicit solver [5]. In order to remain closer to the static implicit response with the fully incompressible formulation, a value of $D_1 = 0.05$ is attributed, as well as a coefficient value of $C_{10} = 1.0$, for an acceptable ratio K_0/μ_0 of 20. It establishes the set of nearly incompressible parameters, that offers a good compromise for the total CPU elapsed time. A third model is also proposed with the nearly incompressible parameters to study the implications of a softer bulk response for the implicit solver. These model setup variants for each of the striking interfaces are contrasted in this first analysis step to understand the impact on the output variables of elastomeric door seal simulations.

Compression diagram

Compression diagrams are generally built as a function of seal deflection by measuring the compression force per sealing length [12]. Usually, seal manufacturers hold on to compressive loads to define the seal design that corresponds to operational characteristics for the seal application. Analogously, the striker interfaces are compared for the set of seal-striker models during 2s on a linear compression loading step.

From preliminary results, with a fully incompressible formulation, the seal compression diagram is used to define at which seal deflection from the flat surface striker has a similar linear load as the C-channel striking interface. Then, the nearly incompressible model variants are compared to verify whether the compression diagrams present any influence on the relevant output results. Figure 6 presents the model results of the seal compressed shape for each striker geometry, where the resultant reaction forces on the reference point are divided per length of the seal to build the diagrams.

Figure 7 presents the collection of diagrams from each striker interface as functions of the seal material formulation and solver scheme[3].

The smaller bulk modulus of the nearly incompressible formulation is less evident for relative smaller seal deflections on loading diagrams, as the results with the flat surface suggest. Comparisons between implicit and explicit solutions in the quasi-static analysis of rubber-like materials [21] demonstrate how the degree of confinement influences the results depending on the loading speed and the rubber compressibility. The study recommends that, for proper quasi-static approximation with the explicit solver, the ratio between kinetic energy (ALLKE) and internal energy (ALLIE) should remain bellow 1% to be comparable to the static implicit solution. Figure 8 shows how the energy ratio evolves for each model during 2s explicit analysis.

[3] Imp. for implicit and Exp. for explicit.

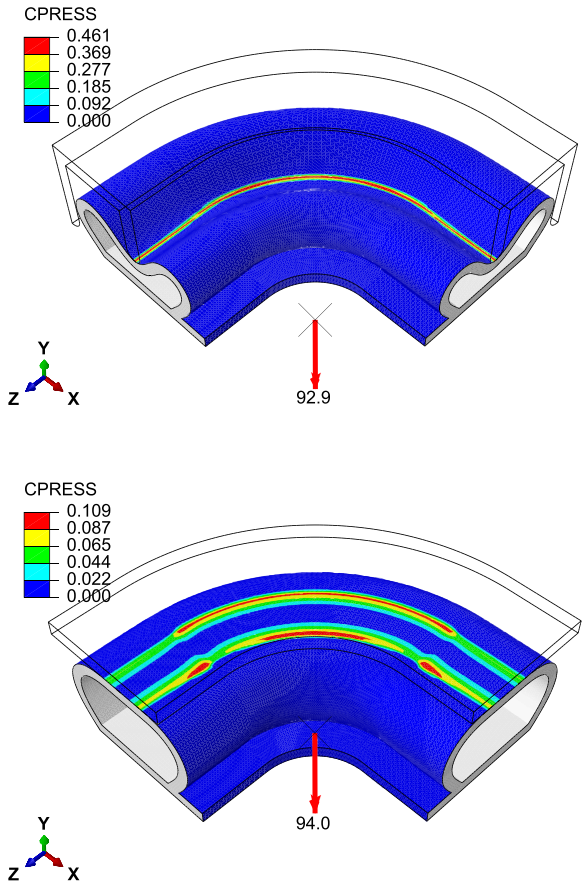

Fig. 6 Seal compression results for full incompressibility

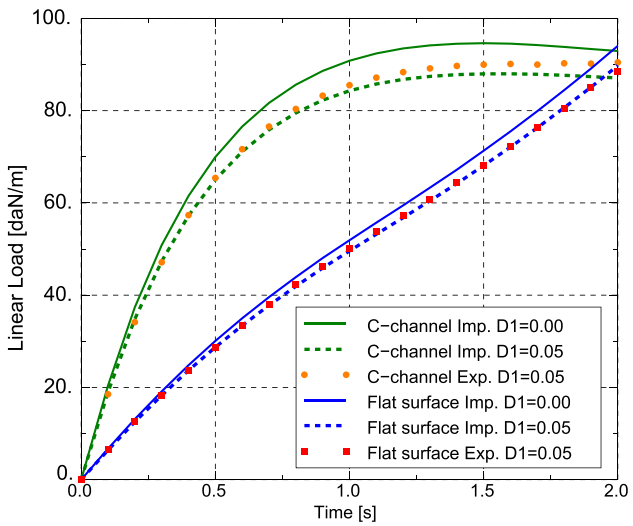

Fig. 7 Compression diagram of each interface and model

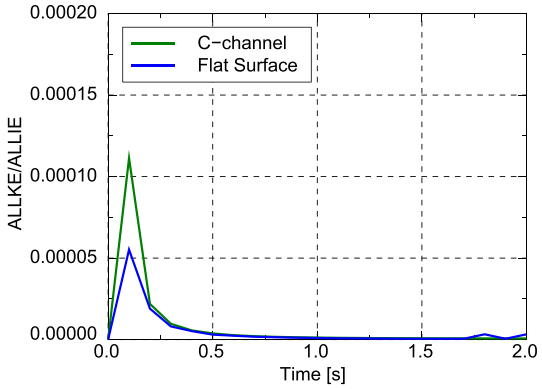

Fig. 8 Energy ratio between kinetic and internal energy

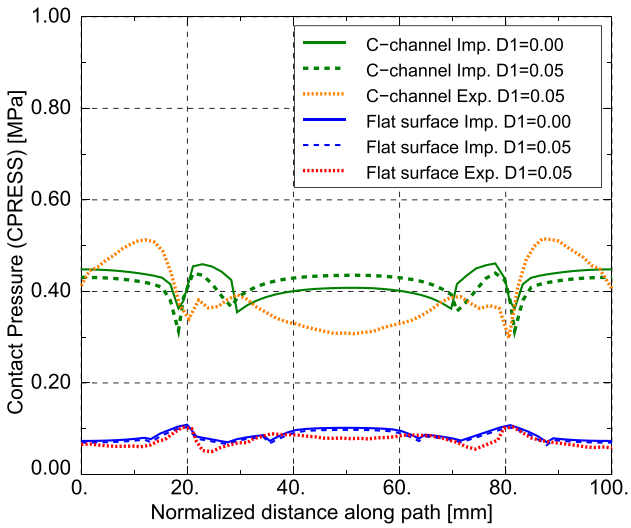

Fig. 9 Contact pressures along the normalized node path

Contact pressure

Although the compression diagrams are similar for each model, the quasi-static approximation used for the explicit solution can present variations of contact results compared to the corresponding static solution of the implicit solver. In Fig. 6, the contour plot illustrates how the contact pressures are established at the end of the seal compression. The connected node paths that present contact values on the seal surface define the sealing lines which are seen as the boundaries for cabin pressure. While the C-channel geometry has a unique sealing line with higher contact pressures due to smaller contact areas, the flat surface presents two major lines with relative lower contact pressure magnitudes.

Figure 9 shows the contact pressure of the sealing lines established at the end of the compression load step for each model configuration. For the flat surface, only the first sealing line, closer to the cabin area, is evaluated, since it is the first boundary for the cabin pressure. The contact pressure

Table 4 Summary results of the seal compression problem

C-channel Solver	Load (daN/m)	CPRRES Max (MPa)	CPRRES Min (MPa)
Imp. $D_1 = 0.00$	94.0	0.461	0.354
Imp. $D_1 = 0.05$	88.0	0.440	0.314
Exp. $D_1 = 0.05$	90.5	0.515	0.298
Flat surface Solver	**Load (daN/m)**	**CPRRES Max (MPa)**	**CPRRES Min (MPa)**
Imp. $D_1 = 0.00$	94.0	0.109	0.070
Imp. $D_1 = 0.05$	89.8	0.104	0.064
Exp. $D_1 = 0.05$	88.6	0.103	0.050

output (CPRESS) is plotted as a function of the normalised distance along the sealing line node path of approximately 100mm.

The plotted results highlight the influence of the bulk modelling of the seal and the difference between the static and quasi-static approaches. The minimum and maximum pressure peaks can be shifted because of the incompressibility constraint, as it is observed between implicit models. However, the quasi-static explicit approach can be more sensitive as the compression loads for higher degrees of confinement. For example, the contrast between explicit simulations is more pronounced for the C-channel as for the flat surface.

Summary of the seal compression problem

Table 4 summarises all seal compression simulation results at the end of this first load step for each rigid interface. The maximum and minimum peak values of the contact pressure (CPRESS) are compared between the solver results. The equivalent Poisson ratio $\nu = 0.475$ is associated to the nearly incompressible rubber formulation with analysis parameters D_1 and C_{10} according to Eq. (17). For the next analysis step considerations under cabin pressure, the seal compression results are essential for the pressure load definition.

Experimentally, all materials are compressible with typical unfilled rubber-like materials having Poisson ratios very close to 0.5. The recommended D_1 value for the explicit solver brings the analysis results to a nearly incompressible behaviour near the range of filled elastomers, with K_0/μ_0 between 50 and 200 [5]. Results show how compressibility influences the seal response, but also how quasi-static approach impacts the contact pressures rather than the resultant linear loads on the compression diagram. The sealing lines originated from contact distributions play a vital role in the seal leak mechanism, since they delimit the initial boundary conditions for cabin pressure problem. If the model is not able to simulate the seal bulk response properly, inaccurate results for air leakage analysis should be expected.

By assuming close minimum contact values after seal compression on each model, the nearly incompressible material formulation is employed in the following analysis. Even though the fully incompressible rubber constraint is mostly recommended for compression problems, especially when the seal is very confined, the nodal force balance of the seal profile is hardly achieved with implicit solutions under cabin pressure, to be described in Sect. 5. Thus, cabin pressure simulations are conducted conservatively, considering that lower contact pressures may impair the sealing effect.

Pressure load: 2nd loading step

The cabin pressure in the FEM model can be specified as a time-dependent distributed load, which can also rotate in space for geometrically non linear analysis. It requires a set of surfaces (Γ_F), defined as collections of element faces, where the pressure is distributed. However, the established contact domains (Γ_C) initially originated on the previous loading step need to be interactively changed on the definition of the cabin pressure as the seal surfaces located inside the cabin area (Γ_{F_1}) can also change as results of the large deformations.

The elastic leak criterion [8] is used to define the dynamic coupling between surface distributed loads and contact traction constraints to physically represent the air cabin pressure. Essentially, if the seal contact pressures (CPRESS) remain above the fluid current pressure (P) no leakage occurs, so the distributed loads are only prescribed inside the cabin. Figure 10 illustrates, on a 2D coarse mesh of the seal with the C-channel interface, how pressure boundaries are established on the faces of the elements limited by a contact boundary.

It is necessary to mention that this criterion is not absolute for every seal performance investigation. In other

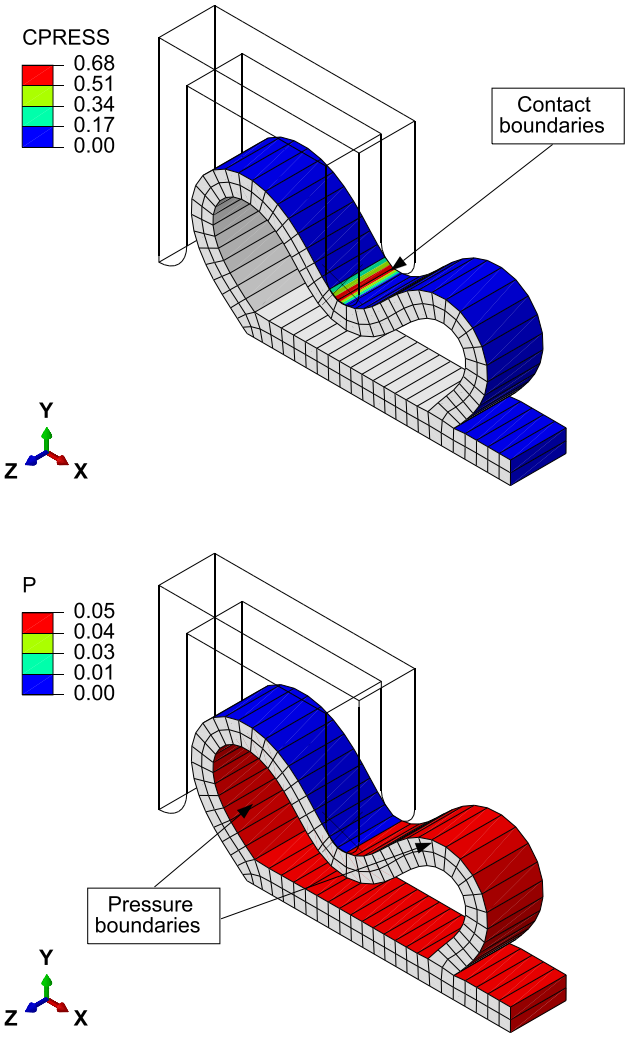

Fig. 10 Contour plot of contact pressure and pressure load respecting the condition of elastic leak of a seal (CPRRES>*P*)

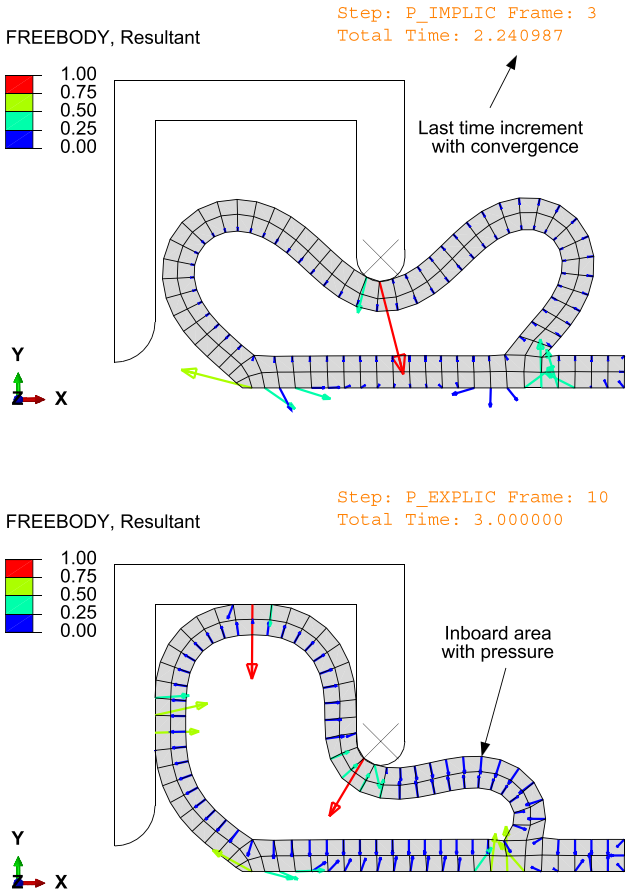

Fig. 11 Nodal resultant forces at last time increment of implicit (top) and explicit (bottom) solvers under pressure load

studies, the leakage mechanism is also described in stages before elastic leak based on the interface roughness and fluid percolation [13]. Nevertheless, the elastic leak failure mode can be useful to evaluate the seal performance qualitatively by taking different seal-striker designs and simulating under the same conditions. Even if the air leakage is not completely measured by this criterion, the moment when the seal starts losing its functionality can be estimated by plotting contact pressures versus cabin pressurisation.

Another failure mode of the seal is the bulb collapse, also useful to understand how the post-leak behaviour affects the seal performance. This criterion is not fully covered by similar studies with CEL technique [9], but its principles are used to evaluate the seal stability under pressure. The necessity of using the explicit rather than the implicit scheme is emphasised by dynamic effects that could start from the sliding mechanism to a complete collapse of the seal profile. On the upper part of Figure 11, the seal instability is presented for the implicit scheme, which requires attention to the convergence issues for the nodal load balance.

The coarse mesh is once more recalled to illustrate the seal collapse at higher flight altitudes. In this case, the seal section is linearly subjected to 0.1MPa over the inboard area during 1s. When friction forces are no longer higher enough then cabin pressure acting over the inboard seal area, the nodal force balance can reach an unstable condition, which is prone for convergence issues for the equilibrium Eq. (13). The last increment, before the implicit analysis ends, occurs at 2.24 s or approximately 24% of one ΔP. Further continuation techniques (Riks method) evidence that structural instability takes place due to stiffness and contact loss.

Figure 12 presents the evolution of load proportionality factor (LPF) from the Riks [5] implicit analysis for the pressure load step of the C-channel, showing a bifurcation point after 30% of pressure load application. Despite not being detailed in this work, the Riks method is referenced as an analysis solution for unstable non linear static problems involving post-buckling behaviour. The concept of time is replaced by the "arc length" measurement to calculate

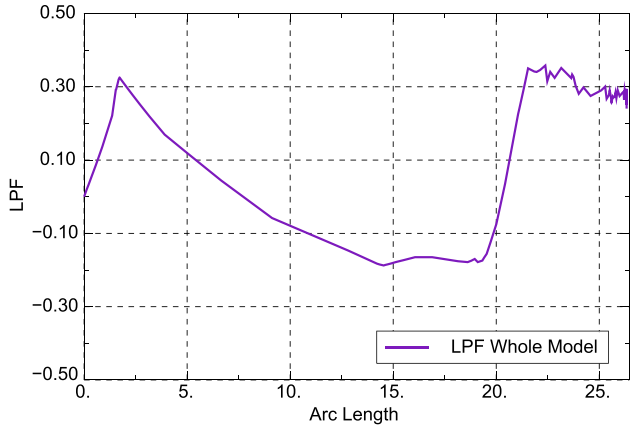

Fig. 12 Risk analysis load proportionality factor attempts

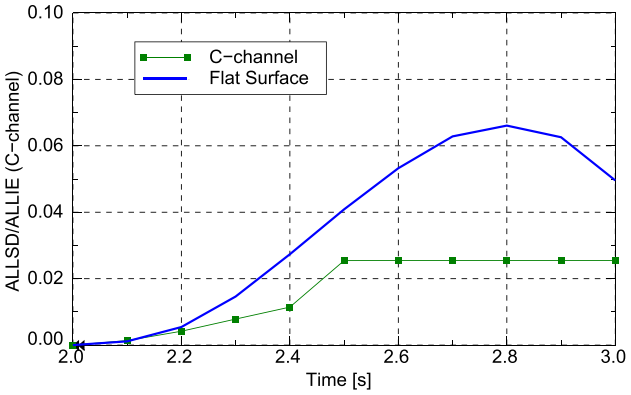

Fig. 14 Model stabilisation energy ratio required for each interface for FPP application between 2 s and 3 s step time

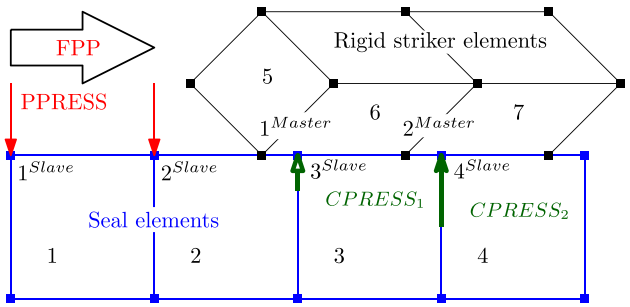

Fig. 13 Schematic representation of FPP contact interaction

the progress of the solution based on the equilibrium path between load and displacement, while the progress of LPF shows the magnitude of the pressure load.

When contact loss takes place on post-buckling problems, Riks analysis is not able to find the final solution after some point. ABAQUS manual recommends introducing viscous damping forces to stabilise the static analysis or to rely on system inertia, which is feasible through explicit analysis. On the bottom Figure 11, the 2D seal shows the expected deformed shape after complete cabin pressurisation with the explicit dynamic solution. Unfortunately, the load instability for seal analysis brings other limitations, since the complex pressure distributions on 3D corner model are more feasible with the Fluid Pressure Penetration interaction, which is not available for explicit solutions in ABAQUS.

Fluid pressure penetration (FPP)

For general static implicit analyses, ABAQUS offers an interaction based on contact pairs called Fluid Pressure Penetration (FPP) that allows the simulation of the fluid passing through the surfaces of two contacting bodies. The single slave-node-based penetration of the feature is very robust and can prescribe pressure load for complex seal deformations based on the elastic leakage criteria. This method is also used by other authors [8, 9, 22] for sealing analysis purposes and comparisons with other methods of pressure load prescription.

Figure 13 schematically illustrates how the FPP applies the distributed load pressure (PPRESS) through contact pairs based on contact pressure values from the slave surface elements of the seal. The fluid pressure penetration is applied normally to the slave surfaces following a path from a reference slave node to a master node on the rigid striker elements. If the contact pressure values (CPRESS) are below a defined critical pressure ΔP, the fluid pressure is applied.

Since this functionality is specific for implicit analyses, load instabilities highlighted on the previous section may also occur on the corner of the seal model. To overcome the analysis divergences, contact controls are defined for model stabilisation conditioning. The automatic stabilisation factor of 0.5 and the damping parameter of 0.5 for the tangent fraction are the minimal values found with convergent results for the seal corner. Therefore, the contact controls can deal with the sliding movement and subsequent large rigid body motions from the seal collapse. When the contact is lost, the artificial forces with constant damping factor are added to the equilibrium Eq. (13):

$$\mathbf{P} - \mathbf{I} = c\mathbf{M}^* \cdot \dot{\mathbf{u}}, \tag{18}$$

where $\mathbf{M}^*$ is an artificial mass matrix calculated with unity density, c is the damping factor from the stabilisation parameters and $\dot{\mathbf{u}}$ is the nodal velocities.

This solution may be acceptable for small ratios between the artificial energy dissipation from stabilisation (ALLSD) and the internal strain energy (ALLIE), but there is no common ground about the recommended limits. The best option to judge if automatic stabilisation is suitable

for the air leakage prediction is through experimental validation. Despite presenting a convergent solution, the flat surface is also submitted to the same stabilisation parameters as the C-channel model.

Figure 14 presents how the energy ratios evolve for each striker geometry during the cabin pressure load, between 2s and 3s of analysis time. If the FPP feature detects that contact pressure is under a predefined critical pressure and there is a discontinuity in the sealing line, the fluid pressure is evenly prescribed over all external surfaces, defining the load pressure interval when the air leaks. Despite the load redistribution not being physically representative for post-leakage effects, this first failure mode is helpful to qualitatively compare striker interfaces considering similar model settings.

For the C-channel, it is possible to observe when the pressure load is fully redistributed over the seal: a plateau is created on the energy ratio plot and the sliding movement ceases, so no stabilisation is required after this time increment. The maximum artificial ratio of 2.53% happens when equilibrium is reached at 2.5 s, right after the contact friction loses its intensity. Before leakage, the FPP suppresses the cabin pressure load of the surfaces of the elements that crossed the striker boundary. It contributes to the load instability since the pressure balance between internal and external surfaces starts playing an opposite role for the inflatable seal design. Progressively, contact pressure slowly fades as the seal profile is pushed out of the cabin area, reducing the effectiveness of using positive pressure to increase contact forces when there is altitude gain.

On the other hand, the flat surface presents better performance compared to the C-channel. Despite showing smaller contact pressures on the beginning of cabin pressurisation, the flat geometry has a different interaction regarding the seal response, as the FPP creates open areas where the air/fluid penetrates. New element surfaces are gradually subjected to the cabin pressure as contacts pressures are not high enough to keep the air inside the cabin. Around 2.8 s, a peak ratio of 6.60% for the artificial dissipation is observed, which is a function of the contact friction forces reduction. Although the model is stable up to 0.1MPa, the flat interface tends to lose contact forces and may require automatic stabilisation for larger pressure values.

One complication that could arise by adding automatic stabilisation parameters for static solutions is the errors added to the real seal behaviour. If automatic stabilisation parameters are doubled for the C-channel model, for instance, the ratio of the artificial energy added to the model not only increases but it also modifies the point when the leakage occurs for the C-channel. Figure 15 illustrates the problem, as the solution shifts the leakage point to 70% of the cabin pressure ΔP by adding more artificial energy to the

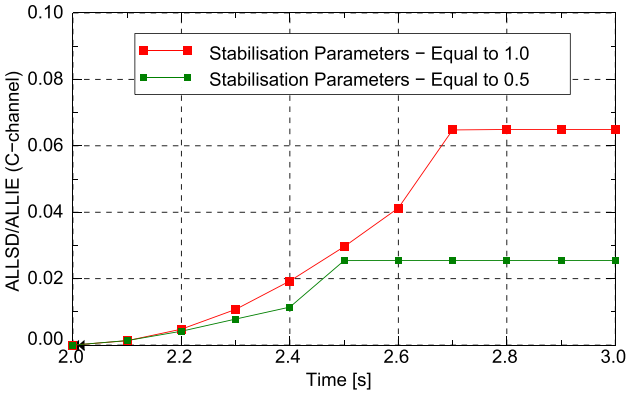

Fig. 15 Influence of the automatic stabilisation parameters

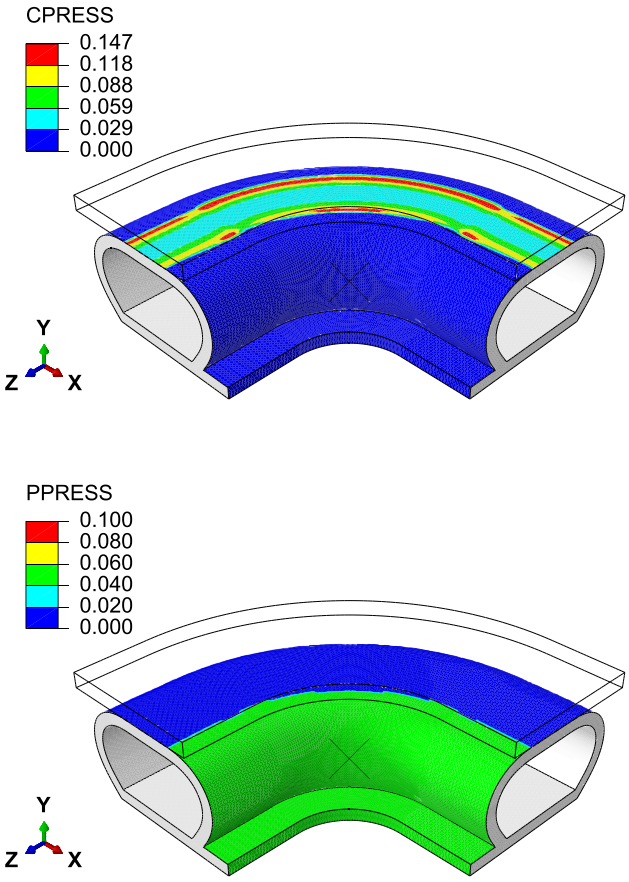

Fig. 16 Flat surface: contact and pressure at 40%ΔP

model. For this reason, experimental validations should be considered to define if the point of leakage is reliable.

Figures 16, 17, 18 and 19 present the contour pressures of each interface designs at 2.4 s and 3 s from the pressure load step. The contour results show that no air leak happens until 40% of the maximum cabin load pressure ΔP is reached for both seal interfaces. Up from this point, each interface

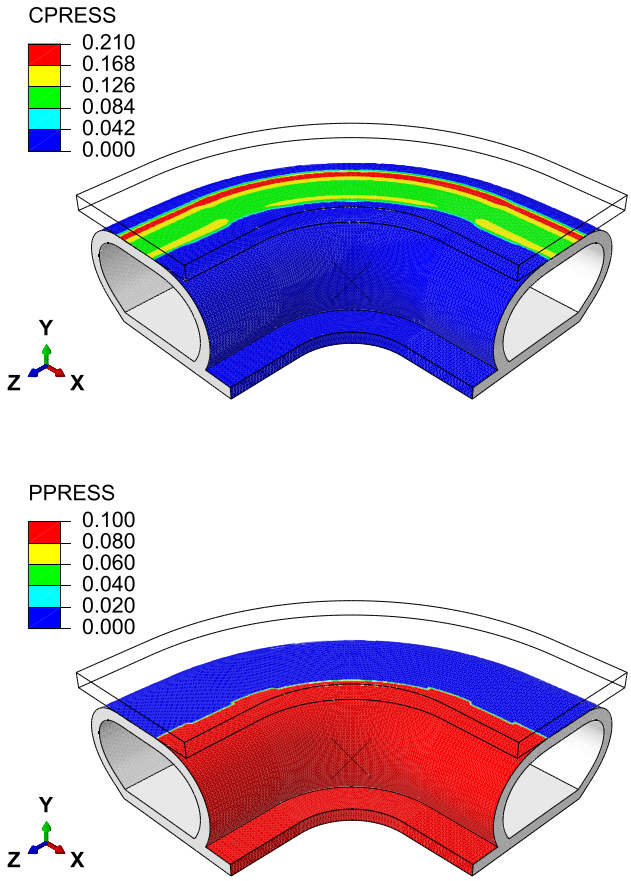

Fig. 17 Flat surface: contact and fluid pressure at 100% ΔP

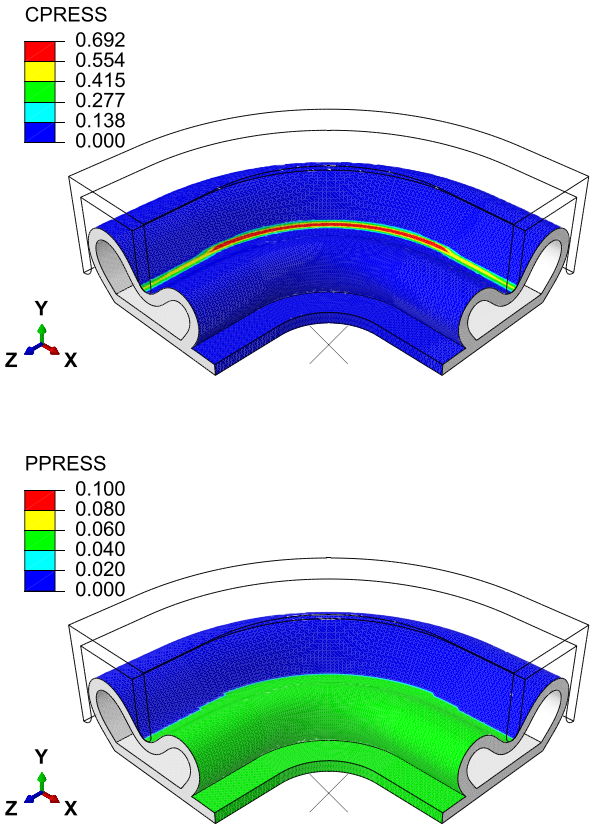

Fig. 18 C-channel: contact and fluid pressure at 40% ΔP

exhibits different results for the fluid pressure (PPRESS) contours. For the C-channel, it is assumed that air leaks at the interval between 40 and 50% of ΔP, while the flat surface can keep the maximum cabin pressure until 3 s of analysis.

User subroutine (DLOAD or VDLOAD)

In the previous subsection, the cabin pressure prescription is based on the first failure mode criterion of the elastic leak, in which the initial contact conditions drive the boundaries of the fluid penetration until a critical contact value is reached. The FPP feature may be not representative for post-leak behaviour of the seal and numerical remedies are required to obtain a convergent solution. The complex interactions between air and seal after leakage should be feasible by combining FEM with CFD [1] or using coupled Euler Lagrangian (CEL) [9], but FSI techniques are not covered by this paper due to long CPU time required for such analysis.

The user subroutines are rather envisaged to simulate the elastomeric seal under cabin pressure beyond FPP limitations with explicit dynamic solutions. By taking advantage of the simplicity of C-channel geometry, this model is used as a candidate to compare the boundary problem with both implicit and explicit solutions. The narrow contact areas of the rigid striker are seen as the unique point of the sealing line where the contact pressure can be reestablished after the seal lost contact. Ideally, the FPP should be able to deliver accurate results if smaller element size and time increments are employed. Preliminary convergence studies showed how the mesh size on the contact areas could interfere with the pressure results.

The proposed strategy is to prescribe the pressure loading from the giving rigid striker coordinates and to impose the pressure only inside of inboard area. DLOAD or VDLOAD subroutines are relatively the easiest subroutines for ABAQUS[4] users to define distributed and concentrated forces for specific applications of non linear load distribution.

Figure 20 illustrates the loading condition can be satisfied for any distributed load subroutine in ABAQUS for the door seal corner model. Points $P^j(x, z)$ represent the sealing line nodes where the contact pressure remains above ΔP, or the critical pressure. The test function $R_j(x, z)$ is derived from

[4] DLOAD for implicit and VDLOAD for explicit scheme.

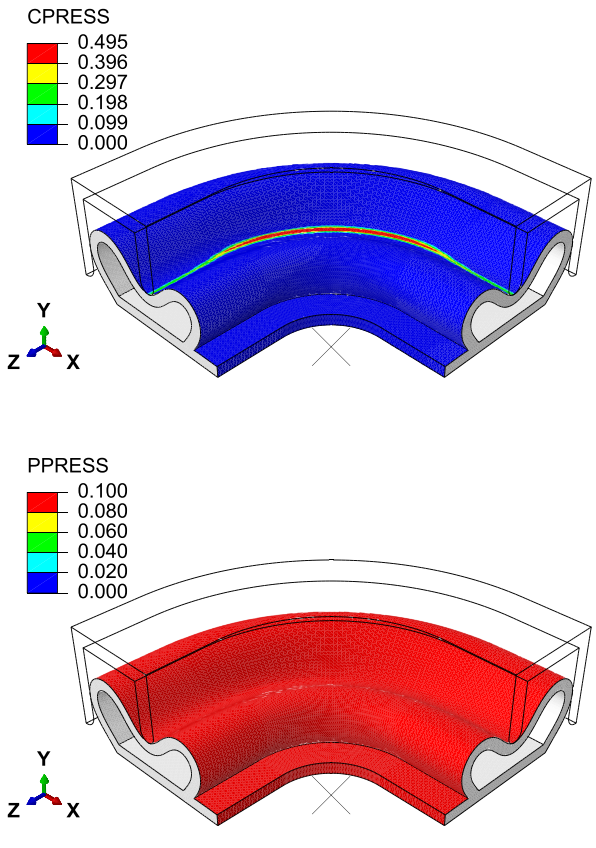

Fig. 19 C-channel: contact and fluid pressure at 100% ΔP

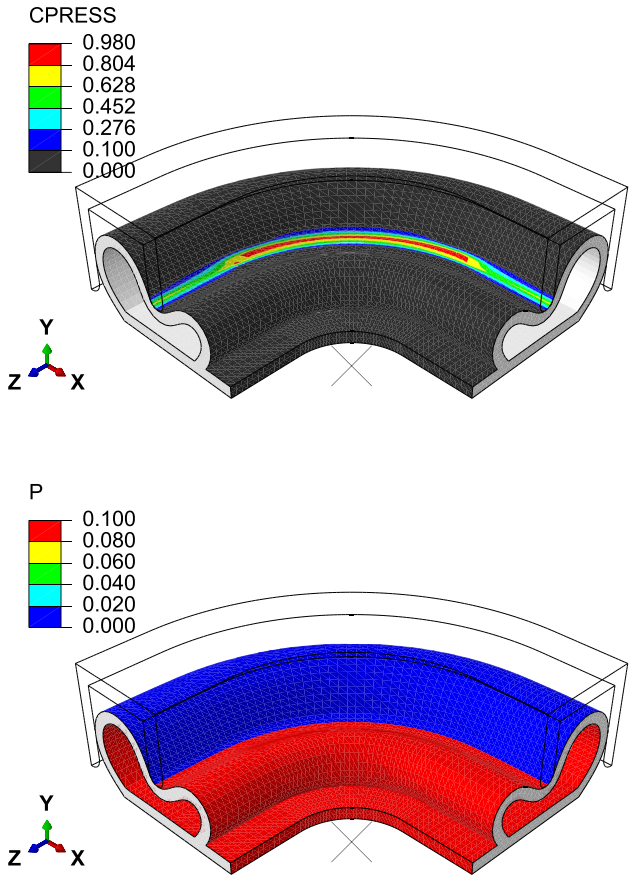

Fig. 21 C-channel with VDLOAD subroutine at 100% ΔP

$$R_j(x,z) = (P_x^{i+1} - P_x^i)(z - P_z^i) - (x - P_x^i)(P_z^{i+1} - P_z^i)$$

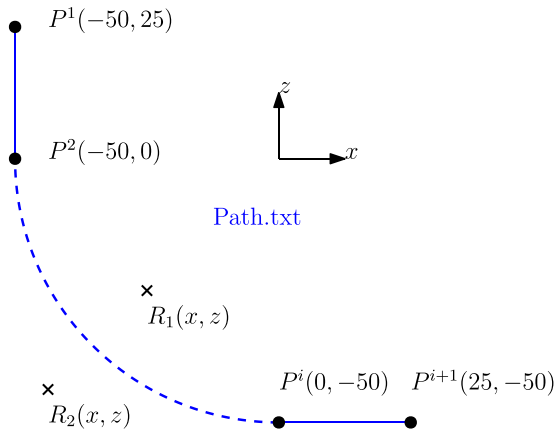

Fig. 20 User subroutine condition for pressure load prescription based on path node coordinates from striker interface

the line equation of each of two consecutive nodal points (P^i and P^{i+1}) that are inside of the node path file (Path.txt), which is read by the algorithm. The current coordinates x and z are generalised for each point j where the load is to be calculated. If the sign of $R_j(x,z)$ is negative or positive, the current pressure for the step time is assigned or not for the surfaces of the elements, respectively. It guarantees that $R_1(x,z)$ is under the cabin pressure, so $R_2(x,z)$ has no value associated with the pressure (zero) giving the predefined striker geometry.

Figure 21 shows the final result of the contact pressure (CPRESS) and pressure load (P) after full pressure. The minimum threshold of 0.1MPa is assigned to the contact pressure contour to contrast the regions where the values are above the maximum value of cabin pressure. The VDLOAD related explicit results can be compared to the stabilised static solution with FPP.

The contour plots show the potential of using user subroutines to investigate seal post-leakage effects on door radii. For the specific case of the C-channel interface, the user subroutine has the advantage of imposing distributed loads in a prominent striking position even after the first leakage occurs or the seal loses contact with the interface. On the other hand, it cannot represent the same results obtained for the flat interface with a dynamic sealing line. While the FPP method does not require defining where the sealing

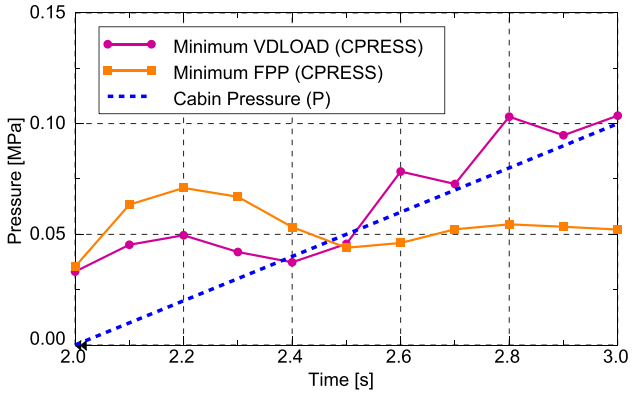

Fig. 22 Contact pressure load and cabin pressurisation evolution for each method on C-channel

line is, the subroutine condition considers a static boundary. The pressure distribution after the leakage should be also dependent on air-fluid dynamics, although user subroutines can be adapted into more physically representative loading conditions on the post-leak. By assuming the small opening areas between seal and striker after short contact loss, the pressure restriction at the narrow edge of the striker can be a good approximation for the real dynamic of the seal. In this case, it is necessary to evaluate if the point of leakage is comparable between FPP and VLOAD. Figure 22 presents the results obtained for the C-channel on each strategy for the minimum value of contact pressure evolution of the sealing lines at intervals of 0.1s of pressure load step.

The last results reinforce that each strategy has a close point of elastic leak and a different response to the post-leak effects. After 2.4 s step time, the minor contact pressure results (CPRESS) are under the actual cabin pressure (P), giving origin to the point where the air leakage occurs. Due to the fixed geometric conditions of the user subroutine and the dynamics of the solution, the seal profile is capable of recovering the sealing effect after 2.6 s, remaining sealed until complete cabin pressure at 3 s. Opportunities for using one strategy instead of the other and further considerations about the analysis results are discussed in the following section.

Conclusion and outlook

The analyses are conducted with qualitative assumptions to simplify the material behaviour and loading cases for air leak performance simulations. During the early stages of flight of cabin pressure, in a quasi-static approach assuming controlled conditions, the isothermal hypothesis is used for the seal compression and cabin pressure loading steps. The seal behaviour is derived from the most basic of the hyperelastic laws of rubber based on acceptable compression limits for standard designs. In contrast, the numerical challenges for the solution are pointed out along with the solver counterpart schemes regarding incompressibility constraint, solution convergence, model stability and the pressure loading definition based on leakage criteria. The following paragraphs present an outlook of the main sections of the door seal analysis.

Section 1 introduces the motivations for the seal analysis under cabin pressure on door corner locations using ABAQUS/CAE 2018 commercial software. The necessity of developing cost-effective door seal solutions emerge from the industrial perspective of the aircraft developing phases. Section 2 presents the relevant studies that helped to define the simulations for seal analysis. Contact and fluid pressure relationships are pointed out on the research as a critical factor for leakage and seal instability. Section 3 establishes the boundary conditions Sect. 3.1 and the main constitutive relations Sect. 3.2 of the elastomeric material and the nearly incompressible nature of the rubber for the FEM seal analysis. Preliminary 2D studies used in Sect. 3.3 settle the optimal mesh size for extrapolated results based on a Grid Convergence Index, which also substantiate the neo-Hookean material law strain limits using prototyping material parameters of rubber. Sect. 3.4 conceives two distinct striking interfaces for the door corner to evaluate the P-shape seal performance with different contact distributions.

Section 4 contains the first analysis results of the door corner and the limitations of dealing with the incompressibility constraint when using an explicit solver. The issues of bringing the implicit solution into convergence need to be considered due to the many problem non linearities. The nearly incompressible behaviour of rubber is addressed as the main protagonist for the seal behaviour since it exhibits close results to the implicit incompressible formulation and the explicit quasi-static approach. Although the differences are accentuated for pressure distributions rather than the linear loads on the compression diagrams, the seal investigations were conservatively performed with smaller contact pressure to start the cabin pressure step.

Section 5 brings more attention to model convergence issues, which are emphasised by the nodal load balance equations that could not be satisfied due to the seal instability, clearly manifested by the Riks method. The analysis in Sect. 5.1 exploited the Fluid Pressure Penetration contact interaction available in the software for specific implicit solutions, with the help of contact automatic stabilisation controls. The main advantage of this contact interaction is the capacity of working for complex interactions between two contact bodies to prescribe physical and representative fluid pressure for the elastic leak criterion. The risks of errors induced by the artificial energy from automatic stabilisation parameters to the solution are mentioned, besides the

fact that the FPP feature is not representative for post-leak observations, such as the seal collapse.

The final analysis in Sect. 5.2 presents an alternative strategy to prescribe the load pressure through VDLOAD user subroutines. Implementable on both implicit and explicit schemes, the load condition of the subroutine takes advantage of the simple striker geometry from the C-channel to impose the boundaries even if a sliding movement takes place. This method is straightforward compared with the previous analysis from FPP regarding elastic leak criterion, with the advantage of not requiring numerical remedies. In fact, defining the correct amount of artificial damping or convenient inertia to the seal instability problem is not a simple task, even if it is the starting point for the proposed study. Thus, experiments that validate the application of each strategy should be further considered to establish the precise point leakage predictions.

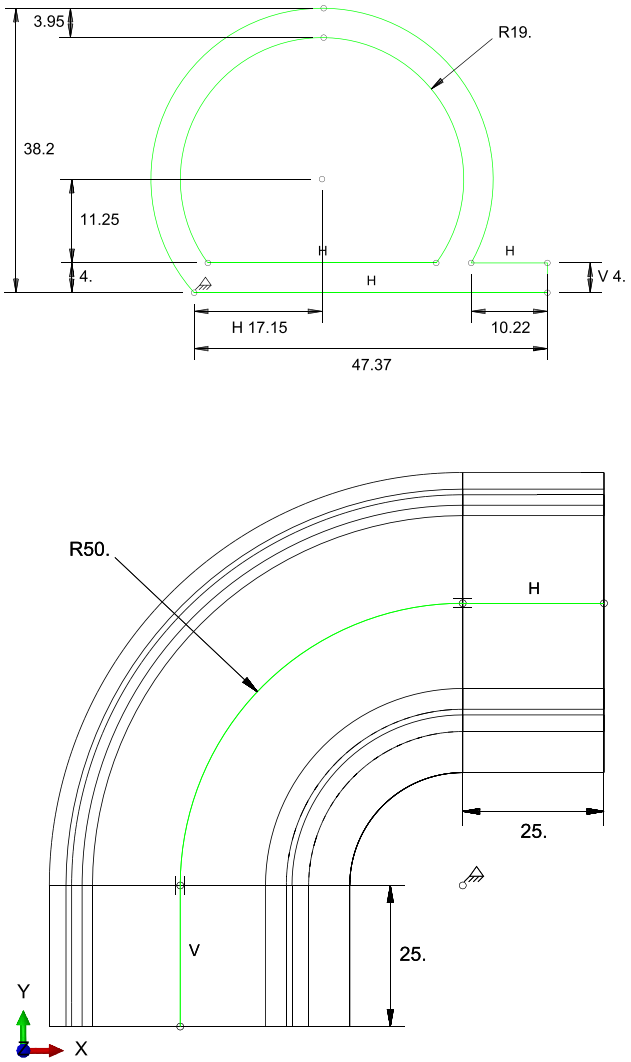

Fig. 23 Sweep cross section dimensions in millimeters (mm)

The simulation strategies presented for elastomeric seal analysis under aircraft cabin pressure exploited native features and simple user subroutines from the FEM commercial software. Although the presented strategies are not able to measure the air leakage rate on the door seals as more advanced techniques with fluid-structure interactions, they offer the benefit of investigating new designs with a relative good time efficiency for each analysis. Through comprehensible material and environment understanding of the boundary conditions, the seal development can be less expansive than trial-error and prototyping measures. For the striker geometries analysed in this work, the C-channel interface proves not to be in an efficient combination with the P-shape seal design, displayed in 7, while the flat surface profits better from the inflatable design solutions to increase contact pressure against air leakage.

Appendix

Figure 23 displays customised aircraft door seal dimensions used to simply represent the cabin pressurization.

Acknowledgements We would like to express our deep gratitude to AIRBUS Operations GmbH in Hamburg.

Funding Open Access funding enabled and organized by Projekt DEAL.

Compliance with ethical standards

Conflict of interest The authors declare no conflict of interest.

References

1. Dong Y, Ke Y, Zheng Z, Yang H, Yao X (2017) Effect of stress relaxation on sealing performance of the fabric rubber seal. Compos Sci Technol 151:291–301
2. EASA: Certification specifications and acceptable means of compliance for large aeroplanes CS-25. Technical Report June, European Aviation Safety Agency (2016)
3. Gorash Y, Bickley A, Gozalo F (2017) Improvement of leak tightness for swellable elastomeric seals through the shape optimization. In: Constitutive models for rubber X—Proceedings of

the 10th European conference on constitutive models for rubber, ECCMR X 2017 (2013), pp 453–458
4. Haupt P (2000) Continuum mechanics and theory of materials. Springer, Berlin
5. Hibbitt K, SI (2018) ABAQUS 2018 theory manual
6. Lacagnina M (2006) Losing the cabin—insights on civil aircraft depressurization. October. Aviation Safety World, pp 33–41
7. Lion A (1997) On the large deformation behaviour of reinforced rubber at different temperatures. J Mech Phys Solids 45(11–12):1805–1834
8. Liu Q, Wang Z, Lou Y, Suo Z (2014) Elastic leak of a seal. Extreme Mech Lett 1:54–61
9. Morrison N, Gorash Y, Hamilton R (2018) Comparison of single-solver FSI techniques for the FE-prediction of a blow-off pressure for an elastomeric seal. ECCM—ECFD 2018 conference (June)
10. Musil B, Johlitz M, Lion A (2020) On the ageing behaviour of NBR: chemomechanical experiments, modelling and simulation of tension set. Continuum Mech Thermodyn 32(2):369–385
11. Niu MCY (1997) Airframe stress analysis and sizing, 3rd edit edn. Adaso/Adastra Engineering Center
12. Parker and Trelleborg (2014) ParFab TM design guide—extruded and hot vulcanized gaskets
13. Persson BNJ, Prodanov N, Krick BA, Rodriguez N, Mulakaluri N, Sawyer WG, Mangiagalli P (2012) Elastic contact mechanics: percolation of the contact area and fluid squeeze-out. Eur Phys J E 35(1):1–17
14. Roache PJ (1994) Perspective: a method for uniform reporting of grid refinement studies. J Fluids Eng Trans ASME 116(3):405–413
15. Rogers W, Armstrong N, Al E (1986) Report of the presidential commission on the space shuttle challenger accident, the cause of the accident. R. Commission. Technical report, NASA, Washington, DC, United States
16. Seal Master Corporation (2018) Precision Built• fully molded elastomers. KENT, OH
17. Sidoroff F (1982) Cours sur les grandes déformations. 51. Sophia-Antipolis
18. Sivakumar V, Palaninathan R (2012) FE analysis of contact pressure prediction on O-rings used in solid rocket booster segment joints. Int J Sci Eng Appl 1(1):8–16
19. Steinmann P, Hossain M, Possart G (2012) Hyperelastic models for rubber-like materials: consistent tangent operators and suitability for Treloar's data. Arch Appl Mech 82(9):1183–1217
20. Parker and Trelleborg (2007) Trelleborg sealing solutions: product range aerospace sealing solutions
21. Yurdabak V, Özüpek Ş (2017) Comparison of the implicit and explicit finite element methods in quasi-static analyses of rubber-like materials. In: Constitutive models for rubber X—Proceedings of the 10th European conference on constitutive models for rubber, ECCMR X 2017, vol 1
22. Zhao B, Zhao YJ, Wu XY, Xiong HC (2018) Sealing performance analysis of P-shape seal with fluid pressure penetration loading method. In: IOP conference series: materials science and engineering, vol 397